Heliyon 10 (2024) e35440

Contents lists available at ScienceDirect

Heliyon

journal homepage: www.cell.com/heliyon

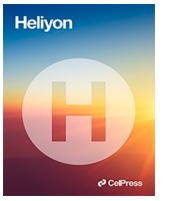

Research article

# Evaluating the image quality and local tumor invasion of uterine cancer by MUSE DWI with RPG

Wenjing Zhao [a], Qing Liu [a], Jining Sun [a], Wenhui Pan [a], Dmytro Pylypenko [b], Wenjuan Wang [a,*]

[a] Department of Radiology, Weifang People's Hospital, Weifang, Shandong, 261041, China
[b] GE Healthcare, Beijing, China

ARTICLE INFO

*Keywords:*
Endometrial cancer
Cervical cancer
Diffusion weighted imaging
Multiplexed sensitivity encoding
Reverse polarity gradient

ABSTRACT

Diffusion-weighted imaging (DWI) is widely utilized for evaluating uterine diseases. However, the prevalent technique, single-shot echo planar imaging (ssEPI), is hindered by notable image distortion and low spatial resolution. Therefore, optimizing uterine DWI sequences is vital for improving image quality. To investigate the efficacy of multiplexed sensitivity encoding (MUSE) combined with reverse polarity gradient (RPG) in enhancing uterine DWI quality and assessing local invasion in endometrial and cervical cancer, we included 149 patients. Each patient underwent DWI of the uterus using ssEPI, MUSE, and RPG-MUSE techniques. We compared these three sequences regarding image quality, signal-to-noise ratio (SNR), contrast-to-noise ratio (CNR), geometric distortion rate (GDR), ADC values, accuracy in determining the extent of cancer invasion, and the Area Under the Curve (AUC) for identifying endometrial cancer and benign endometrial lesions using ADC values. The results indicated that RPG-MUSE DWI had less artifacts than MUSE and ssEPI ($P < 0.05$). Lesions were more apparent in MUSE and RPG-MUSE sequences compared to ssEPI ($P < 0.05$), with RPG-MUSE providing clearer lesion edges ($P < 0.05$). Additionally, RPG-MUSE DWI demonstrated higher SNR and CNR than ssEPI and MUSE ($P < 0.05$), along with a lower GDR ($P < 0.05$). The ADC values did not show significant differences among the three sequences ($P > 0.05$). Furthermore, the AUC of the ROC for detecting endometrial cancer and benign endometrial lesions using ADC values showed no significant differences across the sequences ($P = 0.7609$, 0.7186, and 0.8706, respectively). When combining each DWI sequence with T2WI for FIGO staging, RPG-MUSE and MUSE exhibited better alignment with pathology findings compared to ssEPI ($P < 0.05$). Overall, RPG-MUSE DWI showed fewer artifacts, higher SNR and CNR, reduced geometric distortion, and clearer lesion visualization compared to ssEPI and MUSE, leading to a more precise assessment of endometrial and cervical cancer invasion extent.

## 1. Introduction

Uterine cancers, such as cervical and endometrial, are prevalent in women, with cervical being the fourth and endometrial the sixth most diagnosed [1]. Treatment varies based on the type and extent of the tumor. Thus, accurate diagnosis and assessment of tumor

* Corresponding author.
*E-mail address:* wangwj212@163.com (W. Wang).

https://doi.org/10.1016/j.heliyon.2024.e35440
Received 23 March 2024; Received in revised form 28 July 2024; Accepted 29 July 2024
Available online 30 July 2024

invasion are crucial for selecting the appropriate treatment plan.

Magnetic resonance imaging (MRI) is considered the most effective method for preoperative evaluation of uterine malignancies due to its exceptional ability to provide detailed images of soft tissues and differentiate between non-cancerous and cancerous lesions [2–8]. T2-weighted images (T2WI) are frequently used; however, they can face challenges in detecting certain lesions and accurately delineating tumor margins due to issues like inflammation and vascular congestion [5]. To enhance accuracy, diffusion-weighted imaging (DWI) and dynamic contrast-enhanced (DCE) imaging are incorporated, significantly improving MRI's overall effectiveness in tumor assessment and assisting in treatment planning for uterine tumors [2–5,9].

DWI enhances contrast between tumors and surrounding tissue, improving the accuracy of assessing the size and depth of endometrial and cervical cancers. This is particularly important for patients unable to receive contrast injections or those with isosignal tumors on contrast-enhanced images [2,5,9–11]. Conventional DWI uses single-shot echo-planar imaging (ssEPI), which allows for fast imaging and motion insensitivity. However, this method is hindered by image blurring due to prolonged echo times and is susceptible to artifacts and geometric distortions [11], limiting its spatial resolution. While parallel acquisition techniques can reduce these distortions and blurring, there are still inherent limitations [3,12]. As a result, assessing uterine tumors with conventional DWI, such as determining tumor size or parietal or vaginal invasion, can be challenging due to the low spatial resolution and geometric distortions [13].

The multiple-shot DWI technique reduces image blurring and geometric distortion compared to conventional ssEPI DWI. However, strong diffusion-sensitive gradients can cause phase changes between shots, leading to severe artifacts if data are reconstructed directly. Various reconstruction schemes now mitigate these effects, maintaining high image quality despite tissue motion [12,14,15]. General readout segmentation techniques, which use 2D navigators for phase correction, reduce motion effects between shots [9,14]. Interleaved, phase-segmented methods also minimize motion impacts through two-dimensional navigational echoes [15]. Navigator-less techniques, such as multiplexed sensitivity encoding (MUSE), employ conventional sensitivity encoding to assess and correct motion-induced phase variations. This approach enhances scan time and acquisition efficiency, reduces blurring and distortion in DWI images of various body parts, and improves signal-to-noise ratio (SNR) and resolution, resulting in clearer anatomical details [16]. Furthermore, this technology provides superior image quality in endometrial cancer DWI compared to reduced field-of-view techniques [17], and it can seamlessly integrate with other technologies to further improve DWI image quality [16].

Another method to reduce distortion is the reverse polarity gradient (RPG) method [18,19]. By leveraging the distortion symmetry of B0 inhomogeneity, images in forward and reverse phase-encoded trajectories are collected at $b = 0$ s/mm$^2$, and distortion field maps are computed to correct the entire diffusion dataset [19]. Unlike conventional techniques that acquire static B0 distortion maps separately, extending scan time, the RPG-MUSE technique integrates RPG into MUSE DWI, achieving high-resolution, high spatial fidelity DWI without increasing scanning time [18]. RPG-MUSE acquires lens images interleaved in opposite phase encoding directions, using the estimated distortion map for correction. This method significantly reduces geometric distortion in cranial, head, and neck DWI compared to SS-EPI and MUSE [18,20,21].

Currently, no research has yet explored RPG-MUSE in uterine DWI. Given its promising results in other studies, we hypothesize that RPG-MUSE could significantly enhance uterine DWI image quality. This study implements RPG-MUSE in uterine DWI to assess its efficacy in improving image quality, determine its utility in evaluating localized invasion in endometrial and cervical cancers, and

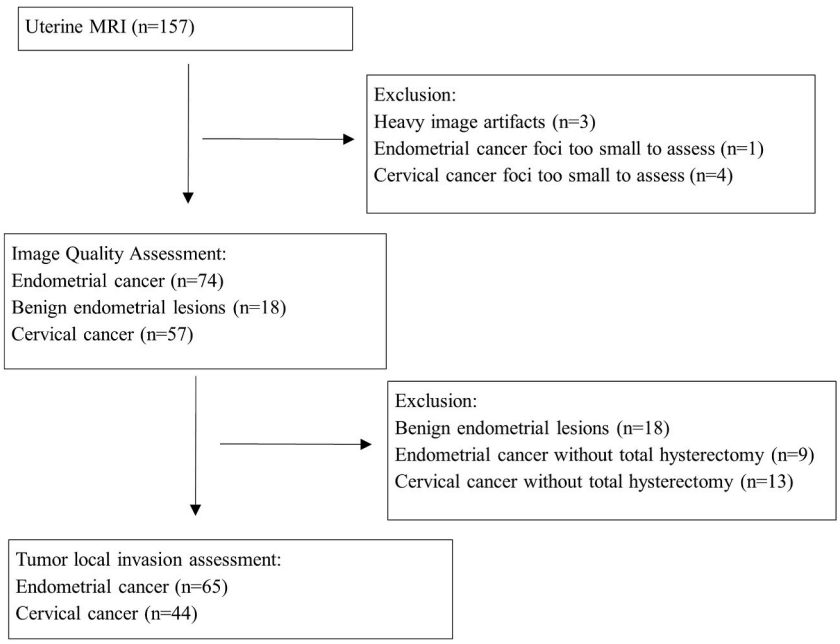


**Fig. 1.** Patient recruitment process.

compare its effectiveness with ssEPI and MUSE sequences.

## 2. Materials and methods

### 2.1. Patients

The Medical Research Ethics Committee of Weifang People's Hospital approved the study protocol (KYLL20231101-3), and a waiver for informed consent was received. Patients who underwent uterine MRI from October 2022 to October 2023 at our hospital were recruited. The inclusion criteria were: 1) MRI examination for uterine disease, 2) pre-treatment evaluation for endometrial cancer, 3) pre-treatment evaluation for cervical cancer. The exclusion criteria were: 1) patients with claustrophobia who could not cooperate with the magnetic resonance examination, 2) patients with metallic implants such as intrauterine devices, pacemakers, and prostheses after hip arthroplasty, 3) patients after radiotherapy, chemotherapy, or surgery for endometrial cancer, 4) patients after radiotherapy, chemotherapy, or surgery for cervical cancer, 5) patients with heavy motion artifacts on the images, 6) patients with cancer foci that were not clearly visible or identifiable on MRI scans and could only be detected through microscopic examination. 157 patients were recruited for uterine MRI examination, excluding 3 cases who could not be evaluated due to heavy image artifacts, 1 case of endometrial cancer foci too small to be evaluated by MRI and 4 cases of cervical cancer foci too small to be evaluated by MRI, and finally of 149 patients were enrolled in this study, including 74 endometrial carcinoma, 18 benign endometrial lesions and 57 cervical cancer. The flow of patient recruitment is shown in Fig. 1.

### 2.2. MRI

Patients were imaged using a GE 3.0T MRI scanner (SIGNA™ Architect, software version DV29.0) equipped with a 30-channel phased array coil (AIR Coil) and a 40-channel bed-integrated coil. All participants were scanned during their non-menstrual period and were required to fast for 4 h beforehand to minimize image motion artifacts by reducing bowel activity. Additionally, patients were instructed to urinate and defecate 30 min prior to the scan to achieve moderate bladder filling.

The standard MRI sequences used included sagittal and axial fat-suppressed T2-weighted imaging (T2WI) and axial T1-weighted imaging (T1WI). For high-resolution imaging, sagittal T2WI and oblique axial T2WI were employed. Diffusion-weighted imaging (DWI) sequences consisted of oblique axial ssEPI, MUSE, and RPG-MUSE.

The parameters for the high-resolution oblique axial T2WI scans were: TR 5874 ms, TE 11.6–231.4 ms, echo spacing 0.7 ms, slice thickness 3.5 mm, slice spacing 0.5 mm, 24 slices, field of view (FOV) 240 × 240 mm, matrix size 352 × 240, pixel dimensions 0.7 × 1.0 mm, frequency direction A/P, ASSET factor 1.5, and NEX 2, with a total scan time of 2 min and 4 s. The parameters for the DWI scans are provided in Table 1. Activating the RPG option on the control panel allowed for the acquisition of two sets of images—MUSE DWI and RPG-MUSE DWI—without increasing the overall scan time.

The localization lines of the high-resolution T2WI and DWI sequences were identical, both in oblique axial position and perpendicular to the uterine lesions. That is, the localization line was perpendicular to the endometrium for endometrial lesions and perpendicular to the cervix for cervical lesions.

### 2.3. Image analysis

The MRI images were analyzed on a GE post-processing workstation (AW4.7). The READYView software provided by the vendor automatically generated ADC maps from the DWI images. Three radiologists, with 12, 20, and 21 years of experience in abdominal imaging, respectively, conducted qualitative evaluations. For the quantitative analysis, two radiologists (evaluator 1 with 12 years and

**Table 1**
The scanning parameters for DWI.

| | ssEPI | MUSE DWI | RPG-MUSE DWI |
|---|---|---|---|
| Number of shots | 1 | 2 | 2 |
| TR (ms) | 4459 | 4866 | 4866 |
| TE (ms) | 75.2–144 | 77.6–160 | 77.6–160 |
| Echo spacing (ms) | 0.7 | 0.7 | 0.7 |
| Slice thickness (mm) | 3.6 | 3.6 | 3.6 |
| Slice spacing (mm) | 0.4 | 0.4 | 0.4 |
| Number of slices | 24 | 24 | 24 |
| FOV (mm) | 280 × 280 | 280 × 280 | 280 × 280 |
| Matrix | 132 × 132 | 132 × 132 | 132 × 132 |
| Pixel size (mm) | 2.1 × 2.1 | 2.1 × 2.1 | 2.1 × 2.1 |
| Frequency direction | R/L | R/L | R/L |
| ASSET factor | 2 | 1 | 1 |
| b value s/mm$^2$ | 0, 1000 | 0, 1000 | 0, 1000 |
| NEX | 6 | 6 | 6 |
| RPG | NO | NO | YES |
| Total scan time | 1 min 34 s | 3 min 33 s | 3 min 33 s |

evaluator 2 with 20 years of experience in abdominal imaging) measured the ADC values, with the average of their measurements being used. The radiologists were blinded to the patients' clinical information and the specific DWI sequences used.

#### 2.3.1. Qualitative evaluation

The images were evaluated by three radiologists for susceptibility artifacts, lesion saliency, and clarity of lesion edges based on a 5-point Likert scale, respectively, as shown in Table 2.

#### 2.3.2. Quantitative evaluation

Regions of interest (ROI) were outlined on the uterine lesion, myometrium (or cervical fibrous stroma), and background (refers to the air area), respectively, at the same scanning level, and the ROIs were copied and pasted onto the b = 1000 s/mm$^2$ images of all DWI sequences, and the signal intensity (SI) and standard deviation (SD) of the corresponding ROIs were measured. SNR = $SI_{lesion}$/$SD_{background}$. Contrast-to-noise ratio (CNR) = ($SI_{lesion}$-$SI_{(myometrium\ or\ cervical\ fibrous\ stroma)}$)/$SD_{background}$ [9]. Fig. 2 shows the outline of ROI.

The geometric distortion rate (GDR) was assessed by measuring the deviation of the uterus or cervix maximal diameter in the phase-encoding direction between each DWI sequence (b = 1000 s/mm$^2$) and T2WI. The maximal diameter of the uterus or cervix on DWI was denoted as A, while on T2WI it was denoted as B, with the GDR calculated as GDR (%) = [|A-B|/B] × 100.

### 2.4. Measurement of ADC value

ROIs were initially defined on the DWI images (b = 1000 s/mm$^2$) and then transferred to the ADC maps at the corresponding slice for all DWI sequences to measure ADC values of the lesions. If significant shifts were observed in the DWI images, the ROIs were adjusted accordingly. Care was taken to exclude artifacts, necrotic areas, and cystic regions when outlining the ROIs.

### 2.5. Assessment of the extent of tumor invision

Two radiologists, Evaluator 1 and Evaluator 2, with 12 and 20 years of abdominal imaging experience respectively, jointly assessed the extent of uterine tumor invasion. When disagreements arose, they resolved them through further discussion, which occurred in approximately 16.8 % of cases. To prevent memory bias, each DWI sequence was evaluated with at least a two-week interval. Due to the low spatial resolution of DWI sequences, they lacked detailed anatomical information. Therefore, T2WI was used as the anatomical reference for assessing the local extent and margins of uterine tumors, with DWI serving as the primary sequence, complemented by T2WI-DWI fusion images (using both cognitive and image fusion). Endometrial and cervical cancers showed higher signal intensity on T2WI, high signal on DWI (b = 1000 s/mm$^2$), and low signal on ADC maps. This study focused solely on the local invasion of the tumor, excluding lymph node and distant metastases.

According to the 2018 International Federation of Gynecology and Obstetrics (FIGO) staging system for endometrial cancer, stage IA indicates that the tumor is confined to the endometrium or infiltrates less than half of the myometrium, stage IB signifies that the tumor infiltrates half or more of the myometrium, stage II denotes that the tumor invades the cervical stroma but does not extend beyond the uterus, and stage IIIA indicates that the tumor invades the serosa of the uterus and/or adnexa. The depth of myometrial infiltration was measured on oblique axial images perpendicular to the endometrium, defined as the distance from the inner edge of the myometrium to the deepest point of tumor infiltration.

For cervical cancer, the FIGO (2018) staging system defines stage IA as invasive cancer visible only under a microscope, stage IB as lesions infiltrating deeper than stage IA, with stage IB1 being 2 cm or less in maximum diameter, stage IB2 being 2–4 cm, and stage IB3 being larger than 4 cm. Stage IIA indicates invasion of the upper two-thirds of the vagina without parametrial invasion, with IIA1 lesions being 4 cm or less and IIA2 lesions being larger than 4 cm. Stage IIB involves parametrial invasion without reaching the pelvic wall [22].

### 2.6. Statistical analysis

Statistical analysis for this study was performed using SPSS 26.0 and MedCalc 21.0 software. Data measurements were presented as mean ± standard deviation (x ± s). The intraclass correlation coefficient (ICC) was used to analyze differences in the qualitative evaluation of image quality between different evaluators, with an ICC >0.75 indicating good agreement [23]. The qualitative evaluation of images, along with SNR, CNR, GDR, and ADC values of the three different DWI sequences, was compared using one-way repeated measures ANOVA, followed by Bonferroni method for pairwise comparisons. The differentiation of ADC values between benign and malignant endometrial lesions was evaluated using a receiver operating characteristic (ROC) curve, and differences in the

**Table 2**
5-point Likert scale.

| | 1 | 2 | 3 | 4 | 5 |
|---|---|---|---|---|---|
| susceptibility artifacts | severe artifacts | more artifacts | moderate artifacts | mild artifacts | no artifacts |
| lesion saliency | difficult to recognize | poor display | display fair | display good | excellent |
| clarity of lesion edges | difficult to recognize | barely recognizable | fuzzy | mildly blurred | clear and sharp |

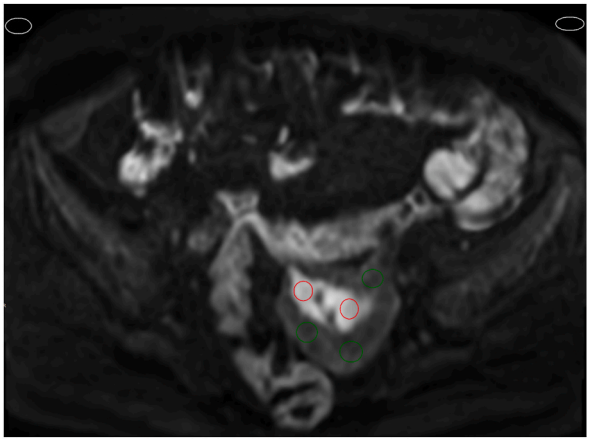

**Fig. 2.** The outline of ROI The red ROI is located on the lesion of endometrial cancer. The green ROI is located on myometrium. The white ROI is located on the air area for noise estimation. (For interpretation of the references to colour in this figure legend, the reader is referred to the Web version of this article.)

area under the curve (AUC) were assessed with the Delong test. The consistency between the extent of uterine malignant tumor invasion, as determined by the three DWI sequences combined with T2WI, and pathological findings was compared using the McNemar's test. A P-value of $<0.05$ was considered statistically significant.

## 3. Results

All patients were pathologically confirmed by uterine biopsy or after hysterectomy, and all patients with FIGO staging by T2WI and DWI underwent total hysterectomy. The interval between total hysterectomy and uterine MRI was not more than one week. The basic data of the patients enrolled in this study are shown in Table 3. 149 patients were enrolled in this study with an age of $53.4 \pm 9.8$ years. They included 74 endometrial cancer, 18 benign endometrial lesions (endometrial polyps or endometrial hyperplasia), and 57 cervical cancer.

The qualitative evaluation of the image quality of the three DWI sequences is shown in Table 4.

There was strong agreement among the three evaluators regarding the susceptibility artifacts in the three DWI sequences, with ICC values of 0.780, 0.762, and 0.824, respectively. The evaluators identified significant differences in susceptibility artifacts across the three DWI sequences ($P < 0.001$), and all pairwise comparisons of the sequences showed statistical significance ($P < 0.001$). All three evaluators consistently found that the RPG-MUSE DWI sequence exhibited fewer susceptibility artifacts compared to the ssEPI and MUSE sequences, as illustrated in Fig. 3(a–d).

Regarding lesion saliency, there was substantial agreement among the evaluators, with ICC values of 0.842, 0.863, and 0.886,

**Table 3**
Information of patients.

| | | number |
|---|---|---|
| Endometrial cancer | total | 74 |
| | pathological subtype | |
| | endometrioid carcinoma | 70 |
| | plasmacytoma | 4 |
| | FIGO staging | 65 |
| | IA | 46 |
| | IB | 14 |
| | II | 4 |
| | IIIA | 1 |
| benign endometrial lesions | total | 18 |
| cervical cancer | total | 57 |
| | pathological subtype | |
| | squamous carcinoma | 49 |
| | adenocarcinoma | 8 |
| | FIGO staging | 44 |
| | IB1 | 11 |
| | IB2 | 19 |
| | IB3 | 7 |
| | IIA2 | 2 |
| | IIB | 5 |

**Table 4**
Qualitative evaluation of image quality.

| Sequence | ssEPI | MUSE | RPG-MUSE | *F* value | *P* value |
|---|---|---|---|---|---|
| susceptibility artifacts | | | | | |
| Evaluator 1 | 2.72 ± 0.67 | 3.12 ± 0.63 | 3.38 ± 0.75 | 89.098 | <0.001 |
| Evaluator 2 | 2.70 ± 0.61 | 3.21 ± 0.66 | 3.44 ± 0.71 | 124.804 | <0.001 |
| Evaluator 3 | 2.69 ± 0.61 | 3.13 ± 0.64 | 3.38 ± 0.70 | 98.926 | <0.001 |
| ICC (95 % CI) | 0.780 (0.724, 0.829) | 0.762 (0.702, 0.814) | 0.824 (0.777, 0.864) | – | – |
| lesion saliency | | | | | |
| Evaluator 1 | 3.38 ± 0.76 | 4.03 ± 0.80 | 4.07 ± 0.79 | 176.753 | <0.001 |
| Evaluator 2 | 3.34 ± 0.77 | 4.02 ± 0.78 | 4.06 ± 0.80 | 211.823 | <0.001 |
| Evaluator 3 | 3.33 ± 0.73 | 4.02 ± 0.75 | 4.07 ± 0.75 | 199.584 | <0.001 |
| ICC (95 % CI) | 0.842 (0.799, 0.878) | 0.863 (0.824, 0.894) | 0.886 (0.853, 0.913) | – | – |
| clarity of lesion margins | | | | | |
| Evaluator 1 | 3.34 ± 0.81 | 3.91 ± 0.80 | 4.04 ± 0.80 | 124.468 | <0.001 |
| Evaluator 2 | 3.29 ± 0.82 | 3.93 ± 0.81 | 4.07 ± 0.79 | 167.215 | <0.001 |
| Evaluator 3 | 3.26 ± 0.77 | 3.89 ± 0.80 | 4.05 ± 0.79 | 160.041 | <0.001 |
| ICC (95 % CI) | 0.815 (0.766, 0.857) | 0.858 (0.818, 0.890) | 0.860 (0.822, 0.893) | – | – |

respectively. The evaluators noted a significant difference in lesion saliency scores among the three DWI sequences ($P < 0.001$). However, no significant difference was observed between the RPG-MUSE DWI and the MUSE DWI sequences ($P = 0.103$, 0.250, 0.156, respectively). Both RPG-MUSE DWI and MUSE DWI sequences received higher scores than the ssEPI DWI sequence ($P < 0.001$). The evaluators agreed that lesions appeared more prominent in the RPG-MUSE and MUSE DWI sequences compared to the ssEPI sequence.

For the clarity of lesion margins, the evaluators showed good agreement, with ICC values of 0.815, 0.858, and 0.860, respectively. They found a significant difference in the clarity of lesion margins across the three DWI sequences ($P < 0.001$), and all pairwise comparisons were statistically significant ($P < 0.001$). The evaluators unanimously agreed that the RPG-MUSE DWI sequence provided the clearest lesion margins, as depicted in Fig. 4(a–d).

The quantitative assessment of the image quality for the three DWI sequences is presented in Table 5. Significant differences were found in the SNR among the ssEPI, MUSE, and RPG-MUSE sequences ($P < 0.001$). Pairwise comparisons between the sequences also showed significant differences ($P < 0.001$), with the RPG-MUSE DWI sequence having the highest SNR.

Similarly, the CNR differed significantly across the ssEPI, MUSE, and RPG-MUSE sequences ($P < 0.001$). All pairwise comparisons were statistically significant ($P < 0.001$), with the RPG-MUSE DWI sequence exhibiting the highest CNR.

The geometric distortion rates also varied significantly among the three sequences ($P < 0.001$). Pairwise comparisons indicated significant differences between the sequences ($P < 0.001$). The RPG-MUSE DWI sequence had the lowest geometric distortion rate, as

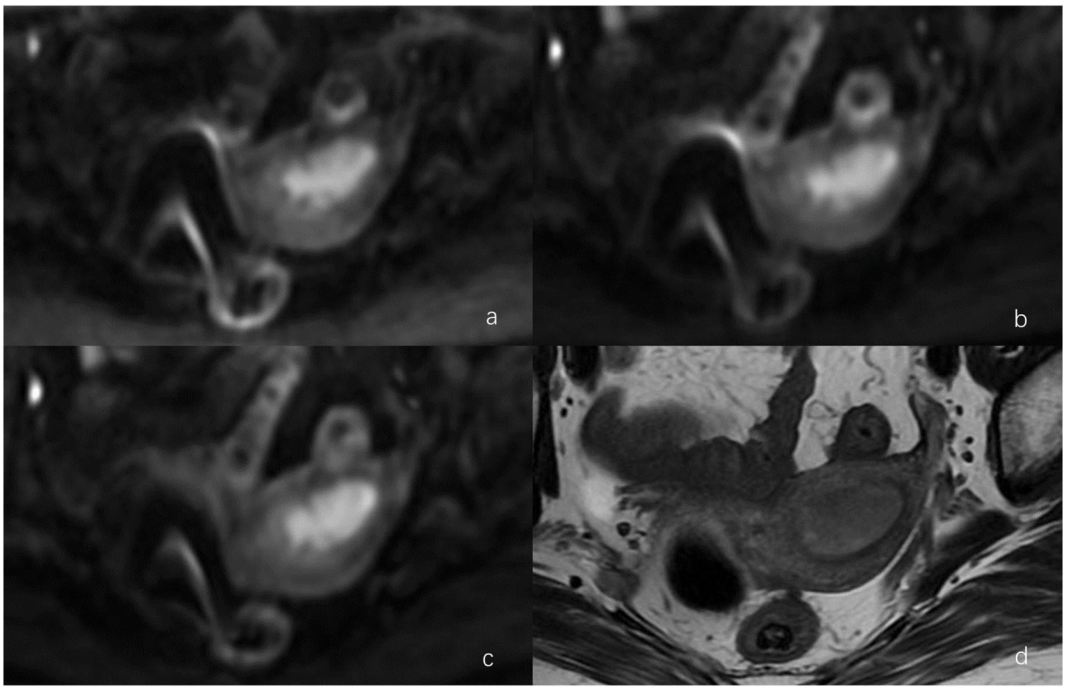


**Fig. 3.** DWI and T2WI maps of patients with endometrial cancer. a) ssEPI DWI, b) MUSE DWI, c) RPG-MUSE DWI, d) T2WI. Among the three DWI sequences, the RPG-MUSE DWI image had fewer artifacts and less anatomical distortion.

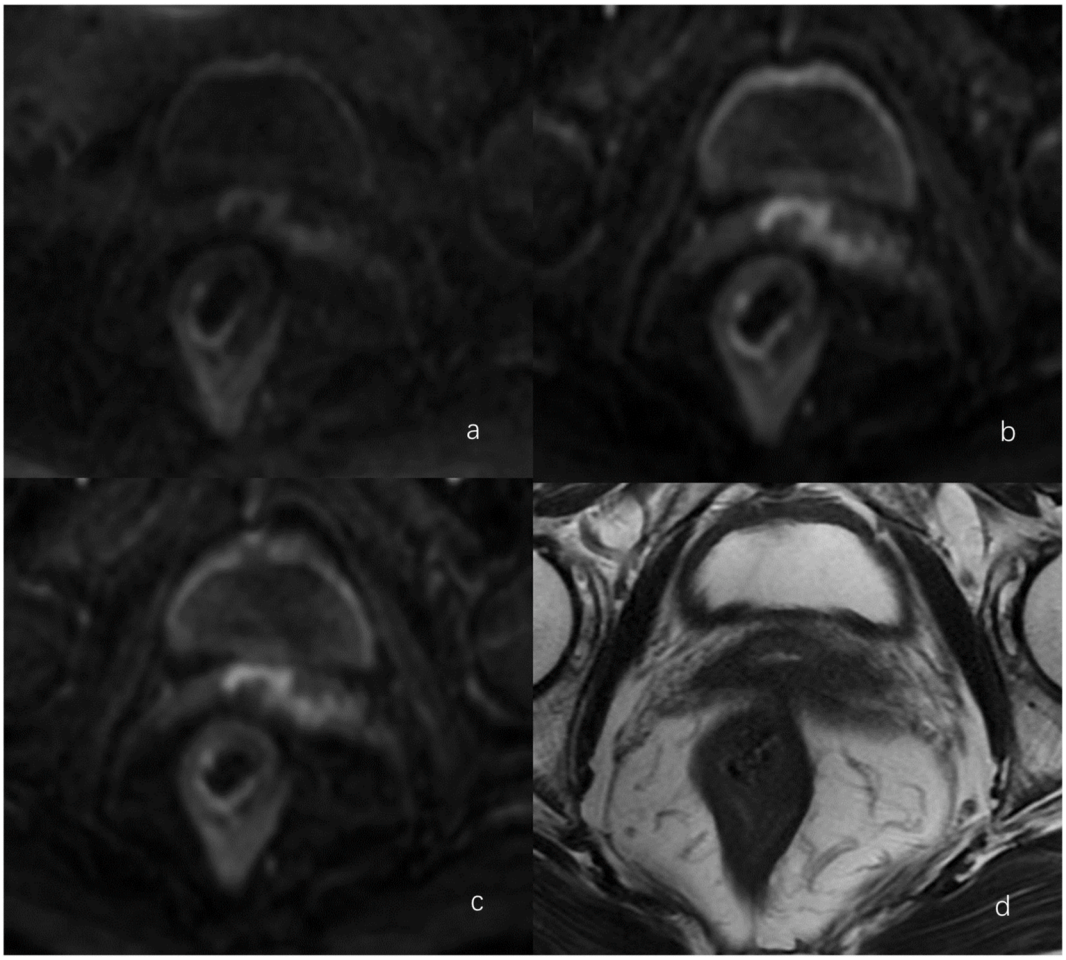


**Fig. 4.** MRI images of cervical cancer involving the vagina. a) ssEPI DWI, b) MUSE DWI, c) RPG-MUSE DWI, d) T2WI. Vaginal cancer foci were poorly visualized on T2WI, and the margins were more clearly shown on RPG-MUSE DWI image.

**Table 5**
Quantitative evaluation of image quality of three DWI sequences.

| Sequence | ssEPI | MUSE | RPG-MUSE | *F* value | *P* value |
|---|---|---|---|---|---|
| SNR | 68.70 ± 34.83 | 247.47 ± 120.53 | 283.19 ± 136.04 | 347.184 | <0.001 |
| CNR | 39.32 ± 25.23 | 143.78 ± 91.16 | 166.88 ± 109.17 | 227.933 | <0.001 |
| GDR | 10.32 ± 5.75 | 7.62 ± 4.88 | 4.95 ± 3.79 | 175.579 | <0.001 |

illustrated in Fig. 5(a - d) and 6(a - d) (see Fig. 6).

Table 6 displays the ADC values for uterine lesions. Analysis revealed no statistically significant differences in the ADC values for endometrial cancer, benign endometrial lesions, and cervical cancer when measured by the three different DWI sequences ($P = 0.191$, 0.760, and 0.900, respectively). The AUCs of the ROC curves for distinguishing between endometrial cancer and benign endometrial lesions using ADC values were 0.977, 0.980, and 0.982 for the three sequences. Pairwise comparisons of these AUC values showed no significant differences ($P = 0.7609$, 0.7186, and 0.8706, respectively). The ROC curve is depicted in Fig. 7.

Table 7 illustrates the FIGO staging data for endometrial cancer. Out of 65 endometrial carcinoma cases, the combination of T2WI with ssEPI, MUSE, and RPG-MUSE sequences aligned with the pathological findings in 48, 55, and 57 cases, respectively. According to the McNemar's test, there were significant differences between MUSE and ssEPI ($P = 0.016$) and between RPG-MUSE and ssEPI ($P = 0.004$), but no significant difference between RPG-MUSE and MUSE sequences ($P = 0.625$). Thus, MUSE and RPG-MUSE sequences demonstrated higher accuracy in staging endometrial cancer than the ssEPI sequence.

Table 8 displays the FIGO staging data for cervical cancer. Among the 44 cervical cancer cases, the combination of T2WI with ssEPI, MUSE, and RPG-MUSE sequences matched the pathological findings in 32, 38, and 39 cases, respectively. Using the McNemar's test, significant differences were found between MUSE and ssEPI ($P = 0.031$) and between RPG-MUSE and ssEPI ($P = 0.016$), while no

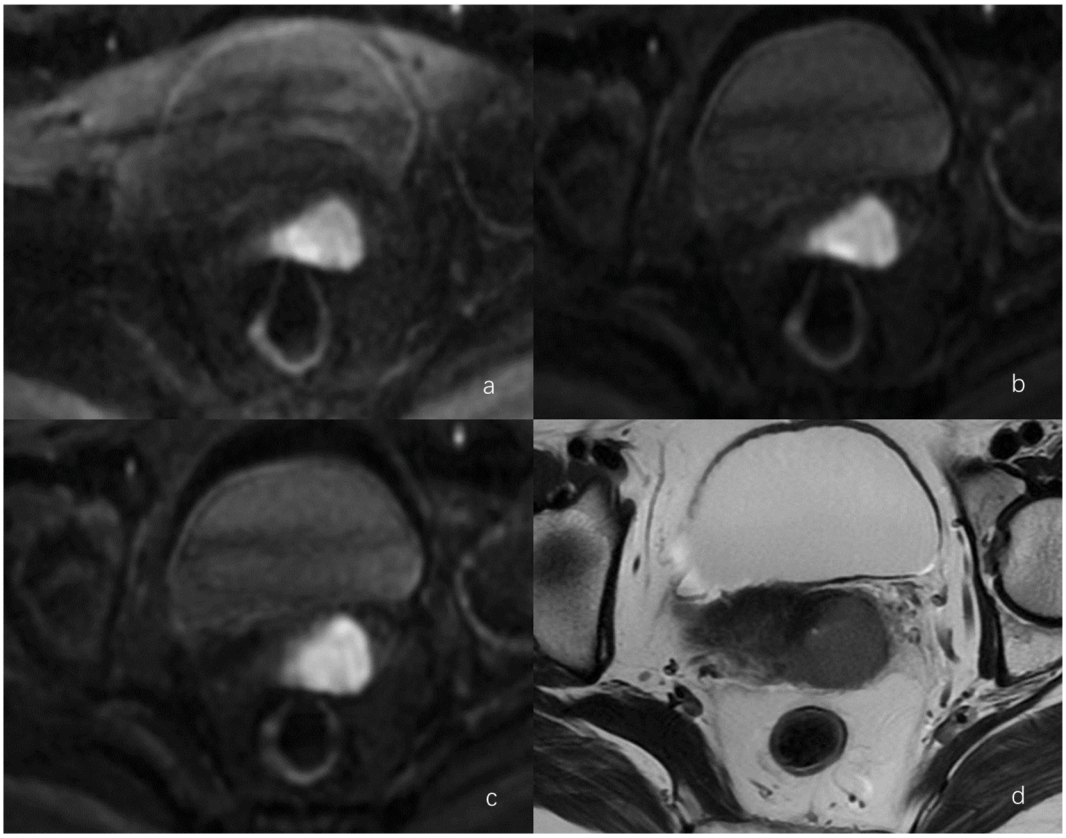


**Fig. 5.** MRI images of a patient with cervical cancer. a) ssEPI DWI, b) MUSE DWI, c) RPG-MUSE DWI, d) T2-weighted. The RPG-MUSE DWI has minimal distortion of the cervical lesions and the rectum, and the anterior border of the rectum is shown more clearly.

significant difference was observed between RPG-MUSE and MUSE ($P = 1.000$). This indicates that the MUSE and RPG-MUSE sequences were more accurate in staging cervical cancer compared to the ssEPI sequence.

## 4. Discussion

This study rigorously compared the image quality of three DWI sequences to determine their efficacy in depicting uterine tumors. RPG-MUSE DWI outperformed both ssEPI and MUSE DWI in reducing susceptibility artifacts and providing clearer anatomical details. While MUSE and RPG-MUSE both significantly improved lesion depiction compared to ssEPI, RPG-MUSE offered sharper lesion margins and clearer edges than MUSE. Previous studies have shown that MUSE reduces blurring and distortion in DWI images of various organs, improves signal-to-noise ratio and resolution, and enhances anatomical detail display [24–31]. Combining MUSE and RPG techniques further reduces geometric distortion and improves DWI image quality [18,20,21]. Our results for uterine DWI were consistent with these findings.

In DWI with high SNR, signal intensity differences between tissues are more pronounced, making lesions easier to identify [9]. This study revealed that combining RPG and MUSE techniques led to improved SNR and CNR in uterine DWI images, better contrast between endometrial and cervical tumors and surrounding normal tissues, and clearer lesion visibility compared to ssEPI and MUSE used individually. MUSE, being a multiple-shot technique, offers advantages over ssEPI by providing higher tissue signal intensity and reduced image blurring due to increased shots and shorter echo chains. Furthermore, MUSE significantly lowers noise levels in DWI, producing higher SNR and CNR compared to ssEPI DWI. Earlier studies have indicated that MUSE enhances SNR, image resolution, and overall image quality in breast DWI relative to ssEPI. Similarly, research by Kim et al. indicated that MUSE-DWI images of the liver have less noise, superior signal-to-noise ratios, clearer visualization of lesions, and improved detection rates. Studies by Chang and Homsi et al. demonstrated that MUSE DWI for intestinal imaging offers higher SNR, better image quality, clearer lesion depiction, and higher diagnostic accuracy than ssEPI DWI. These findings are in agreement with our study, where combining RPG and MUSE techniques resulted in lower background noise and more uniform signals in DWI images, leading to higher SNR and CNR values for RPG-MUSE DWI.

In DWI, image distortions stem from inhomogeneities in the static magnetic field (B0) and gradient eddy currents, with the greatest geometric distortion occurring in the phase encoding direction [21,31]. MUSE, compared to ssEPI, reduces distortion artifacts because of its lower effective echo spacing and higher bandwidth in the phase coding direction [20]. Rakow-Penner et al. found that correcting

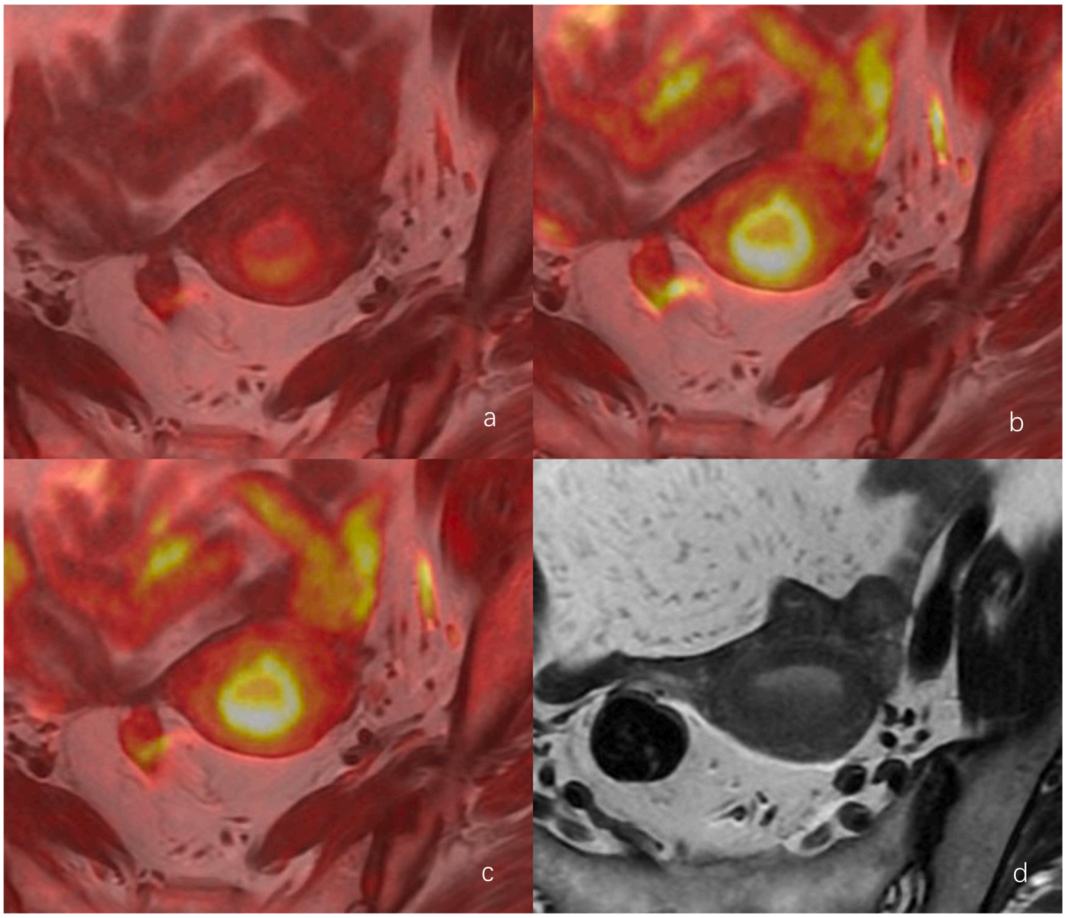


**Fig. 6.** DWI-T2WI fusion maps and T2WI of endometrial cancer (FIGO IA). a) ssEPI DWI-T2WI, b) MUSE DWI-T2WI, c) RPG-MUSE DWI-T2WI, d) T2WI. The margins of the endometrial cancer foci were poorly displayed at T2WI, and the distortion of the cancer foci was the smallest in the RPG-MUSE DWI map among the three DWI sequences.

**Table 6**
ADC values for uterine lesions ($10^{-3}$ $mm^2/s$).

| Sequence | ssEPI | MUSE | RPG-MUSE | *F* value | *P* value |
|---|---|---|---|---|---|
| Endocardial cancer | 0.81 ± 0.15 | 0.82 ± 0.14 | 0.83 ± 0.14 | 1.729 | 0.191 |
| Benign endothelial lesions | 1.27 ± 0.16 | 1.25 ± 0.16 | 1.25 ± 0.15 | 0.276 | 0.760 |
| Cervical cancer | 0.88 ± 0.14 | 0.88 ± 0.15 | 0.88 ± 0.13 | 0.053 | 0.900 |

B0 distortion enhances prostate tumor localization in DWI [19]. Similarly, Bruce and Johansson et al. demonstrated that RPG-MUSE can correct inhomogeneities caused by B0 and gradient eddy currents, reducing geometric distortion in cranial DWI and improving image quality [18,20]. Konar et al. reported that RPG-MUSE significantly reduces distortion and improves spatial accuracy in head and neck DWI compared to ssEPI and MUSE [21]. This study compared the geometric distortion rates of uterine DWI sequences (ssEPI, MUSE, and RPG-MUSE) in the phase encoding direction. Both qualitative and quantitative evaluations indicated that while geometric distortion was not completely eliminated, RPG-MUSE sequences had lower distortion rates than ssEPI and MUSE, further correcting image distortions. Consequently, RPG-MUSE enhanced the overall quality of uterine DWI images. Maintaining high geometric fidelity and adequate spatial resolution is essential for detecting uterine lesions and accurately assessing their size and extent.

As a noninvasive technique, DWI differentiates endometrial cancer from benign lesions like polyps or hyperplasia, with cancers showing lower ADC values [6]. ADC values also help predict tumor grade, stage, and proliferative capacity in endometrial cancer [7], aiding diagnosis and treatment planning, which may improve patient prognosis [6,7]. However, ADC values are influenced by magnetic field strength, scan sequence, and b-value. Studies show RPG-MUSE does not affect ADC measurement in cranial and head and neck DWI sequences [20,21]. In this study, ADC values of endometrial cancer, benign endometrial lesions, and cervical cancer were compared among three DWI sequences, showing no statistical difference. Similarly, no statistical difference was found in AUC values for identifying benign and malignant endometrial lesions using ADC values, confirming that RPG-MUSE does not affect ADC

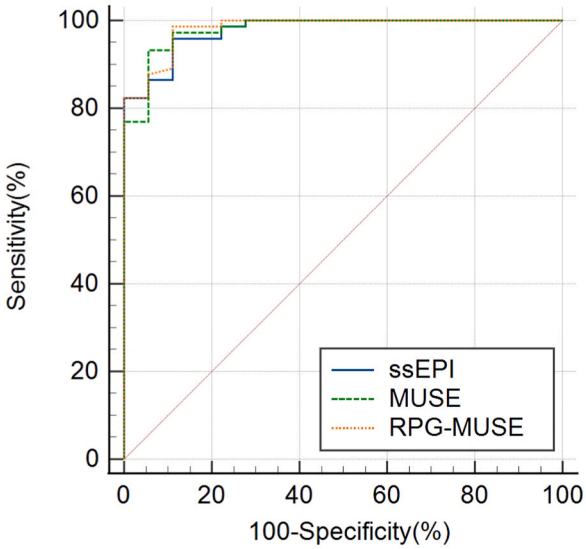


**Fig. 7.** The ROC curve for diagnosis of endometrial cancer with ADC value.

**Table 7**
FIGO staging of endometrial cancer.

| | | Pathological findings | | | |
|---|---|---|---|---|---|
| | FIGO | IA | IB | II | III |
| ssEPI | IA | 36 | 1 | 0 | 0 |
| | IB | 10 | 10 | 2 | 1 |
| | II | 0 | 2 | 2 | 0 |
| | III | 0 | 1 | 0 | 0 |
| MUSE | IA | 40 | 0 | 0 | 0 |
| | IB | 6 | 12 | 1 | 0 |
| | II | 0 | 2 | 3 | 1 |
| | III | 0 | 0 | 0 | 0 |
| RPG-MUSE | IA | 41 | 0 | 0 | 0 |
| | IB | 5 | 12 | 0 | 0 |
| | II | 0 | 2 | 4 | 1 |
| | III | 0 | 0 | 0 | 0 |

**Table 8**
FIGO staging of cervical cancer.

| | Pathological findings | | | | | | |
|---|---|---|---|---|---|---|---|
| | FIGO | IB1 | IB2 | IB3 | IIA1 | IIA2 | IIB |
| ssEPI | IB1 | 9 | 1 | 0 | 0 | 0 | 0 |
| | IB2 | 2 | 15 | 1 | 0 | 0 | 3 |
| | IB3 | 0 | 3 | 6 | 0 | 0 | 1 |
| | IIA1 | 0 | 0 | 0 | 0 | 0 | 1 |
| | IIA2 | 0 | 0 | 0 | 0 | 2 | 0 |
| | IIB | 0 | 0 | 0 | 0 | 0 | 0 |
| MUSE | IB1 | 10 | 1 | 0 | 0 | 0 | 0 |
| | IB2 | 1 | 17 | 0 | 0 | 0 | 2 |
| | IB3 | 0 | 1 | 7 | 0 | 0 | 1 |
| | IIA1 | 0 | 0 | 0 | 0 | 0 | 0 |
| | IIA2 | 0 | 0 | 0 | 0 | 2 | 0 |
| | IIB | 0 | 0 | 0 | 0 | 0 | 2 |
| RPG-MUSE | IB1 | 10 | 1 | 0 | 0 | 0 | 0 |
| | IB2 | 1 | 17 | 0 | 0 | 0 | 1 |
| | IB3 | 0 | 1 | 7 | 0 | 0 | 1 |
| | IIA1 | 0 | 0 | 0 | 0 | 0 | 0 |
| | IIA2 | 0 | 0 | 0 | 0 | 2 | 0 |
| | IIB | 0 | 0 | 0 | 0 | 0 | 3 |

quantification in uterine imaging.

Accurate pre-treatment evaluation of endometrial cancer, including the depth of myometrial invasion and local spread, is essential for tailoring treatment plans [9]. Patients with more than 50 % myometrial invasion have a 6- to 7-fold increased risk of pelvic and para-aortic lymph node metastases, necessitating more aggressive surgical strategies [32]. Combining DWI with conventional MRI sequences such as T1WI and T2WI improves the accuracy of assessing endometrial cancer size and infiltration depth [2,9]. Gas in nearby intestinal tubes can cause B0 magnetic field inhomogeneity, leading to susceptibility artifacts and image distortion. This study compared the effectiveness of ssEPI, MUSE, and RPG-MUSE sequences in assessing infiltration depth, using pathological findings as the reference. RPG-MUSE and MUSE sequences demonstrated higher accuracy than ssEPI, likely due to fewer artifacts, reduced blurring, lower geometric distortion, higher resolution, and clearer lesion margins. These high-quality DWI images enhance the depiction of tumor contours and help in accurately determining the extent of endometrial cancer, facilitating better treatment planning.

Accurate assessment of cervical cancer diameter and paracervical invasion is crucial before treatment [5]. Surgical treatment is used for FIGO stages IA, IB1, and IB2, with initial brachytherapy recommended for stage IB2, and simultaneous radiotherapy for stages IB3-IVA [8]. Radical hysterectomy is preferred over total hysterectomy for FIGO stage IB1 in young women wishing to preserve fertility [33,34]. DWI enhances the accuracy of assessing cervical cancer infiltration depth [11] and, when combined with T2WI sequences, reduces variability in the target area for brachytherapy [35]. However, insufficient detail in DWI images can impact diagnostic accuracy. Using pathologically confirmed FIGO staging as a reference, this study compared ssEPI, MUSE, and RPG-MUSE sequences for pre-treatment FIGO staging of cervical cancer. Results indicated that RPG-MUSE and MUSE were more accurate than ssEPI in assessing preoperative FIGO staging. The high-resolution, low-distortion tumor contours provided by RPG-MUSE and MUSE allow radiologists to assess lesion margins and extent with greater accuracy, making them valuable for evaluating cervical cancer before treatment and precisely localizing radiation therapy.

## 5. Limitations of this study

First, this single-center study only included patients who underwent uterine MRI on a single MRI machine within one hospital district, potentially introducing selection bias. Conducting a multi-center study could mitigate this bias by providing a more diverse sample, thereby enhancing the robustness and generalizability of our results. Second, the small sample size, especially among cervical cancer patients, indicates a need for larger studies to confirm our results. Third, the assessment was limited to the oblique axial plane using ssEPI, MUSE, and RPG-MUSE DWI. Including sagittal DWI images could yield more accurate results. Lastly, no drugs were used to suppress bowel peristalsis during imaging, an area that could be improved in future studies to enhance image quality.

## 6. Conclusion

RPG-MUSE DWI outperforms ssEPI and MUSE sequences by offering fewer susceptibility artifacts, higher SNR and CNR, reduced geometric distortion, and improved lesion visualization. These advantages enable a more precise assessment of the infiltration extent of uterine tumors without compromising the evaluation of lesion ADC values. Furthermore, RPG-MUSE DWI improves the accuracy of pre-treatment staging for endometrial and cervical cancer, thereby assisting clinicians in developing suitable treatment plans.

## Ethics statement

This study was reviewed and deemed exempt from informed consent by the Medical Research Ethics Committee of Weifang People's Hospital with the reference number: [KYLL20231101-3], dated [November 1, 2023].

## Data availability statement

Data will be made available on request.

## CRediT authorship contribution statement

**Wenjing Zhao:** Writing – original draft, Formal analysis, Data curation. **Qing Liu:** Resources, Project administration. **Jining Sun:** Visualization, Data curation. **Wenhui Pan:** Validation, Data curation. **Dmytro Pylypenko:** Writing – review & editing. **Wenjuan Wang:** Writing – review & editing, Supervision, Resources, Project administration, Conceptualization.

## Declaration of competing interest

The authors declare that they have no known competing financial interests or personal relationships that could have appeared to influence the work reported in this paper.

## References

[1] H. Sung, J. Ferlay, R.L. Siegel, et al., Global cancer statistics 2020: GLOBOCAN estimates of incidence and mortality worldwide for 36 cancers in 185 countries, CA Cancer J Clin 71 (3) (2021) 209–249.

[2] S. Nougaret, et al., Endometrial cancer MRI staging: updated guidelines of the European society of urogenital radiology, Eur. Radiol. 29 (2) (2019) 792–805, https://doi.org/10.1007/s00330-018-5515-y.

[3] S. Nougaret, et al., From staging to prognostication: achievements and challenges of MR imaging in the assessment of endometrial cancer, Magn. Reson. Imag. Clin. N. Am. 25 (3) (2017) 611–633, https://doi.org/10.1016/j.mric.2017.03.010.

[4] M.M. Otero-García, et al., Role of MRI in staging and follow-up of endometrial and cervical cancer: pitfalls and mimickers, Insights Imaging 10 (1) (2019) 19, https://doi.org/10.1186/s13244-019-0696-8.

[5] Y.K. Matsumoto, et al., Diagnostic accuracy of magnetic resonance imaging for international federation of Gynecology and Obstetrics 2018 IB to IIB cervical cancer staging: comparison among magnetic resonance sequences and pathologies, J. Comput. Assist. Tomogr. 45 (6) (2021) 829–836, https://doi.org/10.1097/RCT.0000000000001210.

[6] Y. Lee, et al., Multiparametric magnetic resonance imaging of endometrial polypoid lesions, Abdominal radiology (New York) 45 (11) (2020) 3869–3881, https://doi.org/10.1007/s00261-020-02567-7.

[7] J.X. Jiang, et al., Endometrial carcinoma: diffusion-weighted imaging diagnostic accuracy and correlation with Ki-67 expression, Clin. Radiol. 73 (4) (2018) 413.e1–413.e6, https://doi.org/10.1016/j.crad.2017.11.011.

[8] L.S. Fournier, A.S. Bats, C. Durdux, Diffusion MRI: technical principles and application to uterine cervical cancer, Cancer Radiother. : journal de la Societe francaise de radiotherapie oncologique 24 (5) (2020) 368–373, https://doi.org/10.1016/j.canrad.2020.02.008.

[9] M. Xie, et al., High resolution diffusion-weighted imaging with readout segmentation of long variable echo-trains for determining myometrial invasion in endometrial carcinoma, Cancer Imag. 20 (1) (2020) 66, https://doi.org/10.1186/s40644-020-00346-7.

[10] M.S. Lee, M.H. Moon, S.Y. Kim, S. Jang, S. Oh, J.Y. Cho, Preoperative risk stratification in women with endometrial cancer: a comparison of contrast-enhanced MR imaging and diffusion-weighted MR imaging, Eur. J. Radiol. 150 (2022) 110276, https://doi.org/10.1016/j.ejrad.2022.110276.

[11] M. Chen, et al., Comparison of reduced field-of-view diffusion-weighted imaging (DWI) and conventional DWI techniques in the assessment of Cervical carcinoma at 3.0T: image quality and FIGO staging, Eur. J. Radiol. 137 (2021) 109557, https://doi.org/10.1016/j.ejrad.2021.109557.

[12] D.A. Porter, R.M. Heidemann, High resolution diffusion-weighted imaging using readout-segmented echo-planar imaging, parallel imaging and a two-dimensional navigator-based reacquisition, Magn. Reson. Med. 62 (2) (2009) 468–475, https://doi.org/10.1002/mrm.22024.

[13] M. Takeuchi, K. Matsuzaki, Y. Bando, M. Harada, Reduced field-of-view diffusion-weighted MR imaging for assessing the local extent of uterine cervical cancer, Acta Radiol. (Stockh.) 61 (2) (2020) 267–275, https://doi.org/10.1177/0284185119852733.

[14] Z. Xu, et al., Technical Note: clustering-based motion compensation scheme for multishot diffusion tensor imaging, Med. Phys. 45 (12) (2018) 5515–5524, https://doi.org/10.1002/mp.13232.

[15] T. Tamada, et al., Comparison of single-shot EPI and multi-shot EPI in prostate DWI at 3.0 T, Sci. Rep. 12 (1) (2022) 16070, https://doi.org/10.1038/s41598-022-20518-8.

[16] N.K. Chen, A. Guidon, H.C. Chang, A.W. Song, A robust multi-shot scan strategy for high-resolution diffusion weighted MRI enabled by multiplexed sensitivity-encoding (MUSE), Neuroimage 72 (2013) 41–47, https://doi.org/10.1016/j.neuroimage.2013.01.038.

[17] T. Ota, et al., Diagnostic accuracy of MRI for evaluating myometrial invasion in endometrial cancer: a comparison of MUSE-DWI, rFOV-DWI, and DCE-MRI, Radiol. Med. 128 (6) (2023) 629–643, https://doi.org/10.1007/s11547-023-01635-4.

[18] I.P. Bruce, C. Petty, A.W. Song, Simultaneous and inherent correction of B(0) and eddy-current induced distortions in high-resolution diffusion MRI using reversed polarity gradients and multiplexed sensitivity encoding (RPG-MUSE), Neuroimage 183 (2018) 985–993, https://doi.org/10.1016/j.neuroimage.2018.09.055.

[19] R.A. Rakow-Penner, et al., Prostate diffusion imaging with distortion correction, Magn. Reson. Imaging 33 (9) (2015) 1178–1181, https://doi.org/10.1016/j.mri.2015.07.006.

[20] J. Johansson, K. Lagerstrand, L. Ivarsson, P.A. Svensson, H. Hebelka, S.E. Maier, Brain diffusion MRI with multiplexed sensitivity encoding for reduced distortion in a pediatric patient population, Magn. Reson. Imaging 87 (2022) 97–103, https://doi.org/10.1016/j.mri.2022.01.003.

[21] A.S. Konar, et al., Diffusion-weighted echo planar imaging using MUltiplexed sensitivity encoding and reverse polarity gradient in head and neck cancer: an initial study, Tomography 6 (2) (2020) 231–240, https://doi.org/10.18383/j.tom.2020.00014.

[22] L. Manganaro, et al., Staging, recurrence and follow-up of uterine cervical cancer using MRI: updated Guidelines of the European Society of Urogenital Radiology after revised FIGO staging 2018, Eur. Radiol. 31 (10) (2021) 7802–7816, https://doi.org/10.1007/s00330-020-07632-9.

[23] J.R. Landis, G.G. Koch, The measurement of observer agreement for categorical data, Biometrics 33 (1) (1977) 159–174.

[24] H.C. Chang, et al., Multi-shot diffusion-weighted MRI with multiplexed sensitivity encoding (MUSE) in the assessment of active inflammation in crohn's disease, J. Magn. Reson. Imag. 55 (1) (2022) 126–137, https://doi.org/10.1002/jmri.27801.

[25] M. El Homsi, D. Bates, Y. Mazaheri, R. Sosa, N. Gangai, I. Petkovska, Multiplexed sensitivity-encoding diffusion-weighted imaging (MUSE) in diffusion-weighted imaging for rectal MRI: a quantitative and qualitative analysis at multiple b-values, Abdominal radiology (New York) 48 (2) (2023) 448–457, https://doi.org/10.1007/s00261-022-03710-2.

[26] Y. Hu, et al., Multishot diffusion-weighted MRI of the breast with multiplexed sensitivity encoding (MUSE) and shot locally low-rank (Shot-LLR) reconstructions, J. Magn. Reson. Imag. 53 (3) (2021) 807–817, https://doi.org/10.1002/jmri.27383.

[27] Y. Bai, et al., MRI: evaluating the application of FOCUS-MUSE diffusion-weighted imaging in the pancreas in comparison with FOCUS, MUSE, and single-shot DWIs, J. Magn. Reson. Imag. 57 (4) (2023) 1156–1171, https://doi.org/10.1002/jmri.28382.

[28] G.C. Baxter, A.J. Patterson, R. Woitek, I. Allajbeu, M.J. Graves, F. Gilbert, Improving the image quality of DWI in breast cancer: comparison of multi-shot DWI using multiplexed sensitivity encoding to conventional single-shot echo-planar imaging DWI, Br. J. Radiol. 94 (1119) (2021) 20200427, https://doi.org/10.1259/bjr.20200427.

[29] I. Daimiel Naranjo, et al., High-spatial-resolution multishot multiplexed sensitivity-encoding diffusion-weighted imaging for improved quality of breast images and differentiation of breast lesions: a feasibility study, radiology, Imaging cancer 2 (3) (2020) e190076, https://doi.org/10.1148/rycan.2020190076.

[30] Y.Y. Kim, M.J. Kim, S.M. Gho, N. Seo, Comparison of multiplexed sensitivity encoding and single-shot echo-planar imaging for diffusion-weighted imaging of the liver, Eur. J. Radiol. 132 (2020) 109292, https://doi.org/10.1016/j.ejrad.2020.109292.

[31] X. Chen, et al., A feasible study on using multiplexed sensitivity-encoding to reduce geometric distortion in diffusion-weighted echo planar imaging, Magn. Reson. Imaging 54 (2018) 153–159, https://doi.org/10.1016/j.mri.2018.08.022.

[32] D.M. Larson, G.P. Connor, S.K. Broste, B.R. Krawisz, K.K. Johnson, Prognostic significance of gross myometrial invasion with endometrial cancer, Obstet. Gynecol. 88 (3) (1996) 394–398, https://doi.org/10.1016/0029-7844(96)00161-5.

[33] N. Bhatla, et al., Revised FIGO staging for carcinoma of the cervix uteri, Int. J. Gynaecol. Obstet.: the official organ of the International Federation of Gynaecology and Obstetrics 145 (1) (2019) 129–135, https://doi.org/10.1002/ijgo.12749.

[34] N. Bhatla, D. Aoki, D.N. Sharma, R. Sankaranarayanan, Cancer of the cervix uteri, Int. J. Gynaecol. Obstet.: the official organ of the International Federation of Gynaecology and Obstetrics 143 (Suppl 2) (2018) 22–36, https://doi.org/10.1002/ijgo.12611.

[35] K. Han, et al., A prospective study of DWI, DCE-MRI and FDG PET imaging for target delineation in brachytherapy for cervical cancer, Radiother. Oncol. 120 (3) (2016) 519–525, https://doi.org/10.1016/j.radonc.2016.08.002.